Vietnam Journal of Catalysis and Adsorption
Tạp chí xúc tác và hấp phụ Việt Nam

http://chemeng.hust.edu.vn/jca/

Synthesis of Mo-Modified TiO_2 Material with Enhanced Photocatalytic activity

Tran Huu Ha, Ngo Van Ngoc, Vo Vien, Nguyen Thi Lan*

Faculty of Natural Sciences, Quy Nhon University, Binh Dinh, VIETNAM
**Email: nguyenthilan@qnu.edu.vn*

ARTICLE INFO

Received: 15/2/2021
Accepted: 11/7/2021
Published: 15/10/2021

Keywords:

TiO_2, MoO_3, photocatalyst, Ilmenite, modified-TiO_2.

ABSTRACT

The Mo-modified TiO_2 was synthesized via facile impregnation combined with pyrolysis of mixtures in several different initial mass ratios of precursors as $m_{Ti(OH)_4}/m_{(NH_4)_6Mo_7O_{24}.4H_2O}$ equaling 5, 10 and 15 in 500 °C for an hour. The as-prepared samples, denoted as n-MT-500 within n for the initial mass ratio of precursors, were characterized by X-ray diffraction, scanning electron microscopy, ultraviolet-visible diffuse reflectance spectroscopy, Raman spectroscopy, as well as X-ray photoelectron spectroscopy, which all not only illustrate the presence of TiO_2 and MoO_3 components in the composites but also demonstrate the introduction of Mo hetero-atom into anatase lattice. All of the obtained samples performed higher photocatalytic activity under visible light than TiO_2 via the photodecomposition of RhB in aqueous solution, in which 10-MT-500 exhibits the highest degradation efficiency up to 87% after 5-hour illumination.

Introduction

Since the first time Fujishima and Honda published their work which inspired many scientists to conduct a variety of researches on the field of applying photo-catalytic activity of semiconductor for resolving global problems such as waste-water treatment, green energy generation, clean synthesis for chemical industry, etc., scientists still devolve themselves to bring these methods from academic investigation to real application. Among oxide semiconductors, titanium dioxide, TiO_2, has attracted much attention of researchers in use as photo-catalyst due to its unique properties such as non-toxicity, low-cost, high photo and chemical stability and so on [1]. However, practical application of pure TiO_2 confronts a number of limitations with two main reasons. Firstly, the wide band gap of approximately 3.2 eV causes that TiO_2 is mainly activated under excitation of photons in UV region which only accounts for about 5% in the solar energy spectrum. In order to overcome this inherent objection, various efforts have been conducted to narrow band gap of TiO_2 via doping hetero-elements [2-4]. Secondly, the low photo-catalytic activity of TiO_2 could be attributed to the high-rated recombination of photo-induced charge carriers. For the purpose of surmounting this disadvantage, the strategy of coupling TiO_2 with other semiconductors, which own appropriate conduction band (CB) and valence band (VB) positions is a promising way to assist separation of photo-generated electron-hole pair then enhance the photo-reactivity of TiO_2 [5-8]. Among oxide semiconductors which are suitable for coupling with TiO_2, molybdenum trioxide, (MoO_3), as one of the most principal layered materials, is an ideal candidate due to its advantages such as high electron-stored ability [9], environmentally

https://doi.org/10.51316/jca.2021.090

friendly as well as relative narrow band gap of 2.85 eV [10] leading to absorption of onset-visible irradiation which is very beneficial for the photo-catalysis.

In this communication, we synthesized the composite of MoO_3/TiO_2 with hierarchical electronic structure via the facile impregnation combined with calcination of precursors. Beside the forming of composites, the as-prepared samples were in a desire of Mo-doping into TiO_2 lattice, due to the smaller radius of Mo^{+6} compared to Ti^{+4}, leading to the reduction of the band gap.

Experiments

Chemicals

Ammonium molybdate tetrahydrate $(NH_4)_6Mo_7O_{24}.4H_2O$ was purchased from China with purity of 99% and used directly without any further modification. Ilmenite ore, as the TiO_2 precursor was collected in Binh Dinh Province, Vietnam.

Decomposition of Ilminite ore, Synthesis of TiO_2 and MoO_3/TiO_2 composites

The direct decomposition of Ilmenite ore collected in Binh Dinh, Vietnam, with chemical compositions presented in Table 1, was conducted via the procedure of Zenghe Li et al.[11] with some modifications. In a typical process, 50 g Ilmenite ore was added into concentrated solution of H_2SO_4 in 500 ml three-necked flask then the mixture was stirred continuously in the range of 200 to 210 °C for an hour. The dark-purple obtained dispersion, as a solution of $TiOSO_4$, was hydrolyzed and the collected precipitate, as $Ti(OH)_4$, was used as Ti precursor for the next steps.

The MoO_3/TiO_2 composite was prepared via impregnation combined with pyrolysis in solid-state. In detail, the constant amount of ammonium heptamolybdate tetrahydrate was added into a 50ml aqueous dispersion of $Ti(OH)_4$ within weight ratios of $m_{Ti(OH)_4}/m_{(NH_4)_6Mo_7O_{24}.4H_2O}$ equaling 5, 10 and 15. The obtained mixtures were stirred continuously at room temperature to evaporate solvent then treated the final solid in 500 °C for an hour. The as-prepared samples were denoted as nMT-500 in which n represents to the weight ratios of precursors. The pure TiO_2 was synthesized by the same procedure without Mo precursor and denoted as TiO_2. For comparison, the collating sample of pure MoO_3 was synthesized by heating separately ammonium heptamolybdate tetrahydrate following the aforementioned process.

Characterization

Powder X-ray diffraction (XRD) patterns of samples were recorded by a D8 Advance X-ray diffractometer with Cu Kα radiation (λ = 1.540 Å) at 30 kV and 0.01 A. X-ray photoelectron spectroscopy (XPS) was obtained by ESCALab spectrometer (Thermo VG, U.K.). The SEM images of samples were recorded on Nova Nano SEM 450. UV-Vis diffuse reflectance spectroscopy (UV-Vis-DRS) was carried out on Cary 5000 (Varian, Australia). Raman spectra were recorded on T64000 Raman with a 633 nm laser as an excitation source.

Photocatalytic Performance

The photo-catalytic activity of all samples was investigated via the photo-degradation of RhB in aqueous solution under visible light irradiation. In a typical experiment, 0.1 g of nMT500 was added into 80 mL RhB solution with the initial concentration of 20 mg/L. The 220V-100W wolfram bulb with UV cutoff filter provided the source of visible light. Prior to irradiation, the suspension was continuously stirred in the dark for 1.5 hours to ensure the establishment of absorption – desorption equilibrium. At every irradiation time interval, about 10 mL of the suspension were taken up then centrifuged to remove the photo-catalyst. The concentration change of RhB was measured at 553 nm wavelength on UV-Vis spectrophotometer (CECIL CE2011).

Results and discussions

Characterization

The XRD patterns of as-prepared samples were presented in Fig. 1. As shown in Fig. 1, the XRD pattern of TiO_2 includes peaks at 2θ = 25.35, 37.9, 48.09, 53.94, 55.06, 62.87, 69.0, 70.4 and 75.3° corresponding to the crystalline planes of (101), (004), (200), (105), (211), (204), (116), (220) and (215) which indicate the well-structured anatase phase of TiO_2 [2, 11-13].

The XRD pattern of collating sample MoO_3 shows peaks at 2θ = 23.4, 25.64, 27.3, 33.86, 39.03 and 49.33° which is consistent with crystalline planes (110), (040), (021), (111), (060) and (002) of orthorhombic MoO_3 (JCPDS Card no. 35-0609) [10], [14]. The nMT500 XRD patterns

also include mainly peak system of TiO_2 anatase phase while the characterizing signals of MoO_3 could be only seen at 23.4 and 27.3°, with weak intensity illustrating the low content of this component, which demonstrates that successful formation of MoO_3 insignificantly alters crystallite structure of TiO_2.

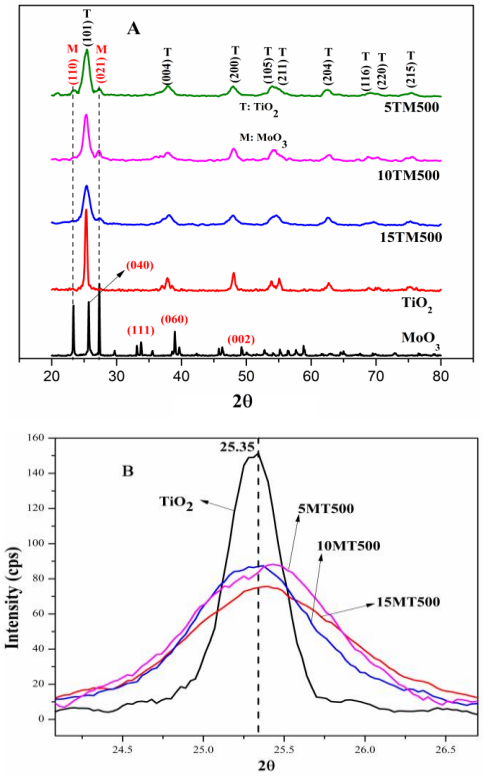

Figure 1: (A) XRD patterns of TiO_2, MoO_3 and nMT500 (n=5, 10, 15); (B) Comparison in intensity, width and red shift of (101) peaks

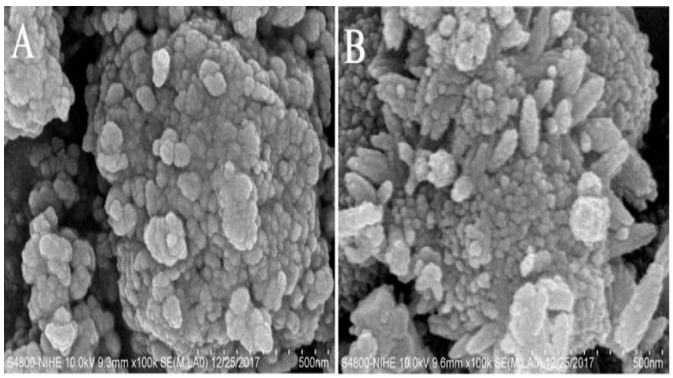

Figure 2: SEM images of TiO_2 (A) and 10MT500 (B)

The low content of MoO_3 in the composites, however, could be assigned to another role of incorporating into the TiO_2 lattice of Mo-element. According to Figure 1A, it is obvious to declare that most of the peaks characterizing for TiO_2 in composite XRD patterns become lower in intensity as well as broader compared to pure TiO_2. Actually, particle size of nMT500 (Table 1) calculated via Debye – Scherrer equation is much smaller than that of bare component which could demonstrate that the introduction of Mo-constituent blocked the growth of TiO_2 particles [15-17].

Table 1: Crystallite parameter and lattice distortion of TiO_2 and nMT500 (n = 5, 10, 15)

Sample	Particles size (nm)	Lattice Parameters			
		d_{101} (nm)	a (nm)	c (nm)	Lattice distortion ε
TiO_2	21.91843	0.350013	0.378878	0.914248	0.011782
15MT500	6.960279	0.350421	0.379101	0.918379	0.041275
10MT500	8.957081	0.350827	0.377989	0.942502	0.036221
5MT500	7.886819	0.351236	0.378211	0.947005	0.047259

This comment was also confirmed by SEM images in Fig 2. Accordingly, beside the existence of rod-liked blocks which could be attributed to the layered MoO_3, SEM analysis of representative 10MT500 shows that, the surface of materials was surrounded by sphere-liked particles of TiO_2 with much smaller size than pure TiO_2.

Furthermore, comparing to pure TiO_2, the highest intensity peak of (101) plane in nMT500 pattern shows a slight red shift to higher 2θ illustrating the effect of inhibiting crystallite growth. Diminution of anatase crystallite quality could be attributed to the change of anatase lattice parameters. In detail, the lattice parameters as *a* and *c* of building unit of tetragonal anatase TiO_2 was estimated by Bragg's law while the lattice distortion *ε* of crystal was inferred via Williamson – Hall equation [18] $\varepsilon = \frac{\beta_{hkl}}{4tan\theta_{hlk}}$ where β_{hkl} is full peak width at half maximum of *(hlk)* plane at angle of θ_{hlk}.

As shown in Table 1, despite the independence of lattice parameter *a*, the *c* lattice constants as well as the interplanar spacing d_{101} values are in direct proportion to the content of Mo-precursor, which could be ascribed to the incorporation of Mo atom into the anatase lattice. As the result of Mo^{+6} radius (0.62 Å) [19] much smaller than Ti^{+4} (0.68 Å) [16]. Mo-atoms could occupy titanium position in crystallite units. In

https://doi.org/10.51316/jca.2021.090

addition, the increase of lattice distortion could be characterized for the introduction of Mo into TiO_2 lattice which could be confirmed in Table 1.

The further investigation on the structure of as-synthesized samples was conducted via Raman spectroscopy which is shown in Figure 3A. The spectra of 10MT500 show the highest peak of Eg signal located at Raman shift of 143.9 cm^{-1} with a slight red shift compared to TiO_2. The other peaks at around 196, 393, 514 and 637 cm^{-1} are corresponding to signals as E_g, B_{1g}, A_{1g} and E_g [20]. The absence of signals for Mo-O bonding combining the above XRD results could deduce the low content of MoO_3.

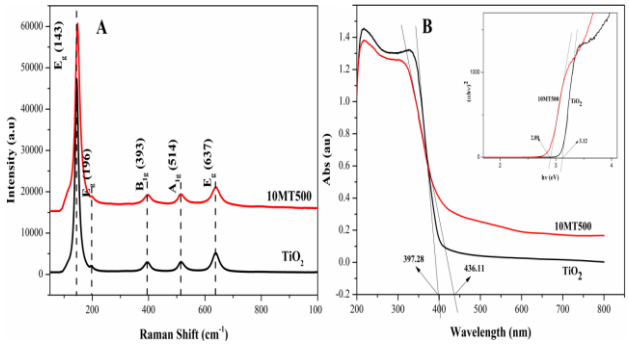

Figure 3: Raman spectroscopy (A) and UV-Vis DRS (B) of TiO_2 and 10MT500

The insertion of hetero-atom was in the desire of narrowing band gap of TiO_2. The reduction of band gap value could be estimated by UV-Vis DRS analysis. As shown in Fig. 3B, the absorbance of representative 10MT500 in visible light region is much higher than TiO_2 which is favorable for photo-catalytic activity. Band gap values of sample were calculated by using Kubelka – Munk function [21] and shown in box of Fig. 3B. The pure TiO_2 exhibits a band gap of 3.12 which concurs with the value of previous reports [2-4], [22]. The modified TiO_2 as 10MT500 performs a clear red shift of band gap energy to around 2.89 eV which could be explained by the formation of charge transfer transition at bottom of conduction band of Mo atom [15-17].

In order to clarify the presence of Mo in as-prepared samples, the XPS analysis had been conducted and shown in Figure 4. Firstly, as shown in Fig. 4A, the Ti2p spectrum of TiO_2 include two peaks at a binding energy (BE) of 459.1 and 464.7 eV which are corresponding to the Ti^{4+} of TiO_2 crystalline [16], [23]. In comparison to the TiO_2, two similar peaks in the Ti2p spectrum of representative 10MT500 located at 459.3 and 465.1 eV, which performs a slight shift to higher BE, indicates the substitution of Mo-atom into anatase lattice [16], [22] Secondly, in Fig. 4B, peaks at 232.4 and 235.6 eV are attributed to BE of Mo^{+6} in which the difference between these peaks is 3.2 eV in agreement with previous reports [24], [25]. The other state of Mo^{+5} could be confirmed by two peaks at 234.6 and 231.6 eV [12], [16]. In addition, the ratio of peak area between Mo^{6+} and Mo^{5+} (3.65) could estimate that the percentage of Mo^{6+} and Mo^{5+} are 78.5% and 21.5%, respectively. That means that most of Mo exists in samples is Mo^{6+}. The presence of Mo^{5+} was an explanation for the aforementioned comment about the significant increase of lattice parameters *a* and *c*, in which most of the previous literatures recommend that due to larger radius of Mo^{5+}[22], [26]. Additionally, the formation of Mo^{5+} could be clarified due to the state of oxygen insufficiency in anatase lattice [22].

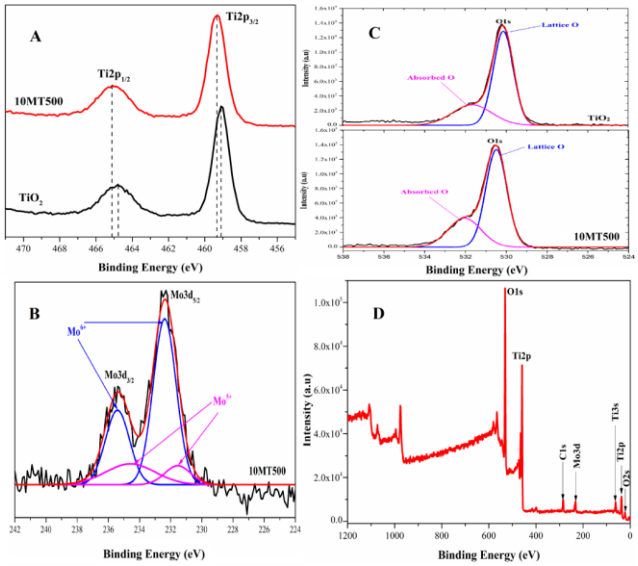

Figure 4: XPS analysis of TiO_2 and 10MT500

The inadequacy of oxygen could be explained via the difference of O1s spectra between TiO_2 and 10MT500. The O1s core level spectroscopy, as shown in Fig. 4C, is the combination of a peak at 530.1 eV, ascribed to BE of anion O^{2-} in TiO_2 lattice, and a slight shoulder at 531.7 eV, related to the form of absorbed oxygen. By contrast, the intensity increase of shoulder could be observed in the O1s spectrum of 10MT500. The increase of absorbed oxygen in modified sample could be clarified due to the deviation in oxygen coordination number of Ti^{4+} and Mo^{6+}[16].

Photo-catalytic activity

Photo-degradation of RhB under illumination of the visible light source was presented in Fig 5. According to the results, all of the modified samples perform higher photodegradation efficiency of RhB than TiO_2 in

https://doi.org/10.51316/jca.2021.090

which 10MT500 exhibits the highest decomposition percentage up to 86.7% after 5-hour visible light irradiation. The enhanced photocatalytic activity of nMT500 compared to TiO_2 could be clarified by parallel effects. Firstly, the insertion of Mo-atom into TiO_2 lattice causes the forming more defects which act as trapping sites to decrease recombination of photogenerated charge carriers. This mechanism was discussed in another previous report of Osmín Avilés-García et al [17]. Accordingly, after being excited to jump through band gap to the conduction band (CB), the photo-induced electron could be trapped by Mo^{+6} to reduce it to Mo^{+5} then extent lifetime of active species. In the next step, electrons could be donated to or trapped by absorbed oxygen or dye molecules to perform its reactivity. The content of Mo-precursors, however, reach an optimal ratio at 10MT500 then the photo-catalytic activity decrease with 15MT500 which could be explained by the fact that the over-increase of defects could lead to forming more recombination sites preventing the performance of active species [22], [27-28].

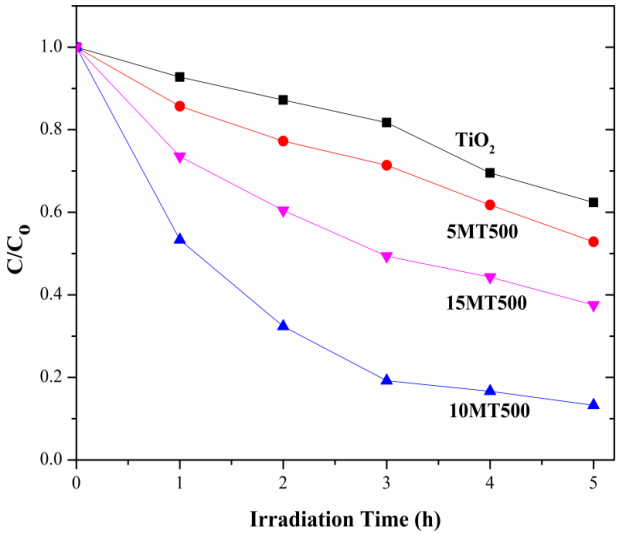

Figure 5: Photo-degradation efficiency of all samples under 5-hour visible illumination

Secondly, the Mo-doping introduce an impurity level in the band gap which is close to the bottom of CB due to the similarity of orbital energy of Mo3d and Ti3d [29] leading to the narrowing its band gap as illustrating by aforementioned UV-Vis DRS analysis. Lastly, the formation of the second semiconductor of MoO_3 could construct a hierarchy energy band structure due to the appropriate CB and VB position of both components. Although pure TiO_2 only activated in the UV region due to its wide band gap [30], band gap between VB of TiO_2 and CB of MoO_3 estimated as 2.6 eV [31], [32] is confirmed that located in the visible region. Therefore, the photo-induced electron could be transferred directly from VB of TiO_2 to CB of MoO_3 though newly-formed Ti-O-Mo bonds [33]. In addition, the Mo-doped TiO_2 with narrower band gap could be activated by photons of onset visible light region to form photo-induced electrons and holes. Hence, the photo-induced electrons could transfer from CB of TiO_2 (-0.25 eV [34]) to more positive CB of MoO_3 (0.52 eV [35]) causing reduction of recombination of photo-induced charge carriers which is beneficial for photocatalysis.

Conclusion

In this work, we report the enhancement in photocatalytic activity of TiO_2 via modification by $(NH_4)_6Mo_7O_{24}$ with facile impregnation synthesis combining heating treatment. All of the characteristic evidences illustrate the role of Mo as hetero-atom inserting in to anatase lattice in the main form of Mo^{6+} beside the small amount of MoO_3 to create heterojunction structure. The results of photo-degradation testing with RhB of all samples demonstrate improvement in photocatalytic activity of modified samples in which the 10MT500 shows the highest efficiency. The mechanism of this enhancement within a few parallel effects had been discussed.

References

1. M. Adachi, Y. Murata, M. Harada, Chem. Lett. 8 (2000) 942–943. https://doi.org/10.1246/cl.2000.942
2. T. Ali, P. Tripathi, Ameer Azam, Waseem Raza, Arham S. Ahmed, Ateeq Ahmed and M. Muneer, Materials Research Express 4(1) (2017) 015022. http://iopscience.iop.org/2053-1591/4/1/015022
3. O. Teruhisa, M. Takahiro, M. Michio, Chemistry Letters 32(4) (2003) 364-365. https://doi.org/10.1246/cl.2003.364
4. J. Wang, D. N. Tafen, J. P. Lewis, Z. Hong, A. Manivannan, M. Zhi, M. Li and N. Wu, J. Am. Chem. Soc. 131 (34) (2009) 12290–12297. https://doi.org/10.1021/ja903781h
5. K.Vinodgopal, I. Bedja, and P. V. Kamat, Chem. Mater. 8 (8) (1996) 2180–2187. https://doi.org/10.1021/cm950425y
6. K. Woan, G. Pyrgiotakis, W. Sigmund, Advanced Materials 21(21) (2009) 2233-2239 https://doi.org/10.1002/adma.200802738

7. J. SukJang, H. Kim, P. H. Borse, J. SungLee, International Journal of Hydrogen Energy 32(18) (2007) 4786-4791. https://doi.org/10.1016/j.ijhydene.2007.06.026
8. Q. Xiang, J. Yu and M. Jaroniec, J. Am. Chem. Soc. 134(15) (2012) 6575–6578. https://doi.org/10.1021/ja302846n
9. Q. Liu, J. Hu, Y. Liang, Z. C. Guan, H. Zhang, H. P. Wang, and R. G. Du, Journal of The Electrochemical Society 163(9) (2016) C539-C544. https://10.1149/2.0481609jes
10. A. Chithambararaj, N. S. Sanjini, S. Velmathi and A. C. Bose, Phys. Chem. Chem. Phys. 15 (2013) 14761-14769. https://doi.org/10.1039/C3CP51796A
11. Z. Li, Z. Wang, G. Li, Powder Technology, 287 (2016) 256–263. https://doi.org/10.1016/j.powtec.2015.09.008
12. N. Boonprakob, N. Wetchakun, S. Phanichphant, D. Waxler, P. Sherrell, A. Nattestad, Jun Chen, Burapat Inceesungvorn, J. Colloid Interface Sci. 417 (2014) 402-409. https://doi.org/10.1016/j.jcis.2013.11.072
13. R.A. Senthil, J. Theerthagiri, A. Selvi, J. Madhavan, Optical Materials 64 (2017) 533-539. https://doi.org/10.1016/j.optmat.2017.01.025
14. I. Shakir, J. H. Choi, M. Shahid, Z. Ali and D. J. Kang, J. Mater. Chem. 22 (2012) 20549. https://doi.org/10.1039/C2JM33458E
15. J. Huang et. al., Hindawi Publishing Corporation Journal of Spectroscopy, ID 681850 (2015) 8 pages. https://doi.org/10.1155/2015/681850
16. S. Wang, L.N. Bai, H.M. Sun, Q. Jiang, J.S. Lian, Powder Technology 244 (2013) 9–15. https://doi.org/10.1016/j.powtec.2013.03.054
17. Osmín Avilés-García, Jaime Espino-Valencia, Rubí Romero, José Luis Rico-Cerda, Manuel Arroyo-Albiter, Reyna Natividad, Fuel 198 (2017) 31-41. https://doi.org/10.1016/j.fuel.2016.10.005
18. V.D. Mote et. al., Journal of Theoretical and Applied Physics (2012) 6(6). https://www.jtaphys.com/content/2251-7235/6/1/6
19. L. Gomathi Devi, B. Narasimha Murthy, S. Girish Kumar, Journal of Molecular Catalysis A: Chemical 308 (2009) 174–181. https://doi.org/10.1016/j.molcata.2009.04.007
20. Fei Kong, Li Huang, Leilei Luo, Sheng Chu, Ying Wang and Zhigang Zou, Journal of Nanoscience and Nanotechnology 12 (2012) 1931–1937. https://doi.org/10.1166/jnn.2012.5163
21. Fattima Al-Zahra, G. Gassim, Ahmed N. Alkhateeb, Desalination 209 (2007) 342–349. https://doi.org/10.1016/j.desal.2007.04.049
22. Matiullah Khan, Junna Xu, Wenbin Cao and Zi-Kui Liu, Journal of Nanoscience and Nanotechnology 14 (2014) 6865-6871. https://doi.org/10.1166/jnn.2014.8985
23. W. K. Jo, T. Adinaveen, J. J. Vijaya and N. C. S. Selvam, RSC Adv., 6 (2016) 10487-10497. https://doi.org/10.1039/C5RA24676H
24. L.E. Firment, A. Faretti, Surface Science 129 (1983) 155-176. https://doi.org/10.1016/0039-6028(83)90100-0
25. T. H. Fleisch, G. J. Mains, Journal of Chemical Physics, 76, 1982, 780-788. https://doi.org/10.1063/1.443047
26. V. Štengl and S. Bakardjieva, J. Phys. Chem. C 114(45) (2010) 19308–19317. https://doi.org/10.1021/jp104271q
27. Batzill M, Morales EH, Diebold U, Influence of nitrogen doping on the defect formation and surface properties of TiO_2 rutile and anatase, Phys. Rev. Lett. 96 (2006) 026103. https://doi.org/10.1103/PhysRevLett.96.026103
28. H. E. Cheng, Y. R. Chen, W. T. Wu, and C. M. Hsu, Nitrogen-doped titanium dioxide (N-doped TiO_2) for visible light photocatalysis, Mater. Sci. Eng. B , (2011) 576-596. https://doi.org/10.1016/j.mseb.2011.02.001
29. Yanqin Gai, Jingbo Li, Shu-Shen Li, Jian-Bai Xia, and Su-Huai Wei, Phys. Rev. Lett. 102 (2009) 036402. https://doi.org/10.1103/PhysRevLett.102.036402
30. H. Mahmood, A. Habib, M. Mujahid, M. Tanveer, S. Javed, A. Jamil, Mater. Sci. Semicond. Process., 24 (2014) 193–199. https://doi.org/10.1016/j.mssp.2014.03.038
31. S. H. Elder et. al., J. Am. Chem. Soc. 122 (2000) 5138-5146. https://doi.org/10.1021/ja992768t
32. A. Q. Khan, S. Yuan, S. Niu, L. Zheng, W. Li and H. Zeng, Optics Express 25(12) (2017) A539-A546. https://doi.org/10.1364/OE.25.00A539
33. H. Liu, T. Lu, C. Zhu, Z. Zhu, Solar Energy Materials & Solar Cells 153 (2016) 1–8. https://doi.org/10.1016/j.solmat.2016.04.013
34. Shelly Burnside, Jacques-E. Moser, Keith Brooks, and Michael Grätzel, J. Phys. Chem. B 103 (43) (1999) 9328–9332. https://doi.org/10.1021/jp9913867
35. Wen Li, Jinfen Chen, Rongting Guo, Jiaming Wu,

Xiaosong Zhou and Jin Luo, Journal of Materials Science: Materials in Electronics 28(21) (2017) 15967–15979.
https://10.1007/s10854-017-7495-0

36. Batzill M, Morales EH, Diebold U, Influence of nitrogen doping on the defect formation and surface properties of TiO_2 rutile and anatase, Phys. Rev. Lett. 96 (2006) 026103.
https://doi.org/10.1103/PhysRevLett.96.026103

37. H. E. Cheng, Y. R. Chen, W. T. Wu, and C. M. Hsu, Nitrogen-doped titanium dioxide (N-doped TiO_2) for visible light photocatalysis, Mater. Sci. Eng. B , (2011) 576-596.
https://doi.org/10.1016/j.mseb.2011.02.001

38. Yanqin Gai, Jingbo Li, Shu-Shen Li, Jian-Bai Xia, and Su-Huai Wei, Phys. Rev. Lett. 102 (2009) 036402.
https://doi.org/10.1103/PhysRevLett.102.036402

39. H. Mahmood, A. Habib, M. Mujahid, M. Tanveer, S. Javed, A. Jamil, Mater. Sci. Semicond. Process., 24 (2014) 193–199.
https://doi.org/10.1016/j.mssp.2014.03.038

40. S. H. Elder et. al., J. Am. Chem. Soc. 122 (2000) 5138-5146.
https://doi.org/10.1021/ja992768t

41. A. Q. Khan, S. Yuan, S. Niu, L. Zheng, W. Li and H. Zeng, Optics Express 25(12) (2017) A539-A546.
https://doi.org/10.1364/OE.25.00A539

42. H. Liu, T. Lu, C. Zhu, Z. Zhu, Solar Energy Materials & Solar Cells 153 (2016) 1–8.
https://doi.org/10.1016/j.solmat.2016.04.013

43. Shelly Burnside, Jacques-E. Moser, Keith Brooks, and Michael Grätzel, J. Phys. Chem. B 103 (43) (1999) 9328–9332.
https://doi.org/10.1021/jp9913867

44. Wen Li, Jinfen Chen, Rongting Guo, Jiaming Wu, Xiaosong Zhou and Jin Luo, Journal of Materials Science: Materials in Electronics 28(21) (2017) 15967–15979.
https://10.1007/s10854-017-7495-0